Received: 27 March 2022 | Accepted: 26 September 2022

DOI: 10.1111/1365-2478.13269

Geophysical Prospecting | EAGE EUROPEAN ASSOCIATION OF GEOSCIENTISTS & ENGINEERS

ORIGINAL ARTICLE

3D reflection seismic imaging of volcanogenic massive sulphides at Neves-Corvo, Portugal

George A. Donoso[1] | **Alireza Malehmir**[1] | **Joao Carvalho**[2] | **Vitor Araujo**[3]

[1]Department of Earth Sciences, Uppsala University, Uppsala, Sweden

[2]LNEG, Amadora, Portugal

[3]Somincor (Lundin Mining), Castro Verde, Portugal

Correspondence
George A. Donoso, Department of Earth Sciences, Uppsala University, Geocentrum, Villavägen 16, 752 36 Uppsala. Sweden.
Email: george.donoso@geo.uu.se

Funding information
European Comission, Horizon 2020, Grant/Award Number: 775971

Abstract

Three-dimensional reflection seismic data from the Neves-Corvo area, southern Portugal, were reprocessed with the main objective of improving the seismic signature of the Lombador and Semblana volcanogenic massive sulphide deposits. The sensitivity for choosing adequate parameters for targeted imaging, even during the pre-processing stage, such as common-depth point binning size, was studied in detail before the main processing work began helping to optimize bin size parameters; preliminary stacking results from this analysis presented severe acquisition footprint, and seismic targets were not clearly identifiable. Processing results using pre-stack dip move-out and post-stack migration methods show strong moderate to steeply dipping reflections. Several of the observed reflections can be correlated with known lithological contacts, some of which are interpreted to originate from the Semblana and Lombador deposits. Despite the mixed signal-to-noise ratio, the seismic cube reveals both shallow and deep three-dimensional structures, allowing to account for the deposits' lateral extension beyond the capabilities of two-dimensional seismic imaging alone. Given the data processing approach taken it was possible to distinguish strong diffraction patterns, interpreted as originating from faults and edges of the Lombador deposit, illustrating the usefulness of diffraction patterns for better interpretation of geological features in hard-rock environments.

KEYWORDS
3D, high-resolution seismic, seismic acquisition, seismic data

INTRODUCTION

High-resolution seismic imaging technologies, already successfully applied in hydrocarbon exploration, have been used in the past decades in mineral exploration to detect and delineate deep-seated deposits, especially volcanogenic massive sulphides (VMS), and their host geologic structures (Eaton et al., 2003; Milkereit et al., 1996, 2000; Urosevic et al., 2012). Early published accounts illustrating the use of seismic methods for direct targeting of mineral deposits come from Africa (Stevenson & Durrheim, 1997 and references therein) and Canada from a series of two-dimensional (2D), three-dimensional (3D), and vertical seismic profile (VSP) surveys (Bellefleur et al., 2004, 2012; Malehmir & Bellefleur, 2009; Matthews, 2002). A successful deep discovery in the Bathurst Mining Camp at New Brunswick, Canada, was a milestone and encouraged follow-up seismic surveys by several companies. At the time Europe was not so far behind, although fewer

This is an open access article under the terms of the Creative Commons Attribution License, which permits use, distribution and reproduction in any medium, provided the original work is properly cited.
© 2022 The Authors. Geophysical Prospecting published by John Wiley & Sons Ltd on behalf of European Association of Geoscientists & Engineers.

13652478, 0, Downloaded from https://onlinelibrary.wiley.com/doi/10.1111/1365-2478.13269 by Cochrane Portugal, Wiley Online Library on [14/12/2022]. See the Terms and Conditions (https://onlinelibrary.wiley.com/terms-and-conditions) on Wiley Online Library for rules of use; OA articles are governed by the applicable Creative Commons License

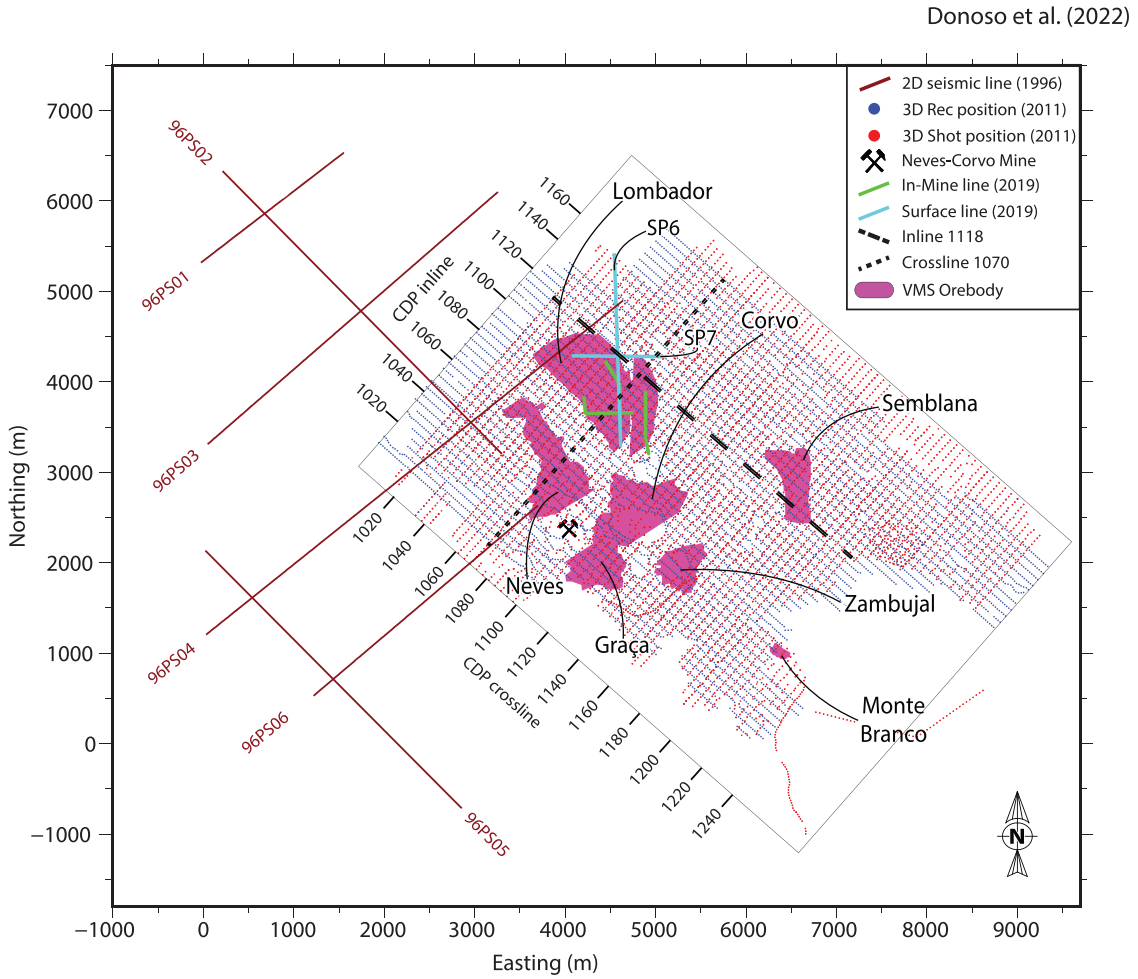

FIGURE 1 Basemap showing the location of the 3D seismic survey relative to the major VMS deposits (magenta surfaces), together with the 1996 2D seismic profiles (red lines), 2019 SP6 and SP7 surface (cyan) and in-mine (green) seismic profiles. The dense blue and red points are receiver and shot positions, respectively, for the 2011 surface 3D seismic survey. The 3D seismic dataset is the focus of this study

studies were published then on the use of seismic methods for mineral exploration. One of the areas where seismic methods were extensively attempted in Europe during the early 1990s and later is the world-class VMS Neves-Corvo in the Iberian Pyrite Belt (IPB), which is the focus of this study.

The VMS deposits located in the Portuguese sector of the IPB have a strong impedance contrast (mainly due to their density) against all lithological host rocks, allowing them to be a good target for the use of seismic methods (Donoso et al., 2020; Yavuz, 2015). Several 2D profiles acquired during the 1990s at the IPB were one of the earliest attempts at employing seismic methods for deep targeting and for structural imaging to better understand the general fault systems in the area. The first useful recorded use of seismic methods for exploration at the Neves-Corvo was done in 1991; however, raw shot gather data are not available for their reprocessing. Later, in 1996, 2D seismic profiles were acquired (Figure 1), allowing to identify and illuminate the northern section of the tier-1 (ca. 150 Mt) world-class Lombador deposit; this 2D legacy dataset was considered to be high fold (96–120 channels per line) at the time of the acquisition and reprocessed by Donoso et al. (2020), obtaining improved results that allowed for visualization of never before seen geological features, validating the usefulness of reprocessing legacy data in this mature mining camp.

In 2011 a 3D surface seismic reflection survey was conducted at Neves-Corvo, covering an area of approximately 24 km^2. This paper presents results from revisiting and reprocessing the 3D surface reflection seismic data while validating the observations against the known deposits. This 3D seismic survey was part of a successful effort to delineate the VMS Semblana deposit (West & Penney, 2017) and to study if additional targets could be found (Yavuz et al., 2015). Additional focus was put on observed diffraction patterns and their importance for defining the shape of VMS deposits. The study of 3D diffraction seismic imaging is well known (Alonaizi et al., 2013 and references therein), and examples from

13652478, 0, Downloaded from https://onlinelibrary.wiley.com/doi/10.1111/1365-2478.13269 by Cochrane Portugal, Wiley Online Library on [14/12/2022]. See the Terms and Conditions (https://onlinelibrary.wiley.com/terms-and-conditions) on Wiley Online Library for rules of use; OA articles are governed by the applicable Creative Commons License

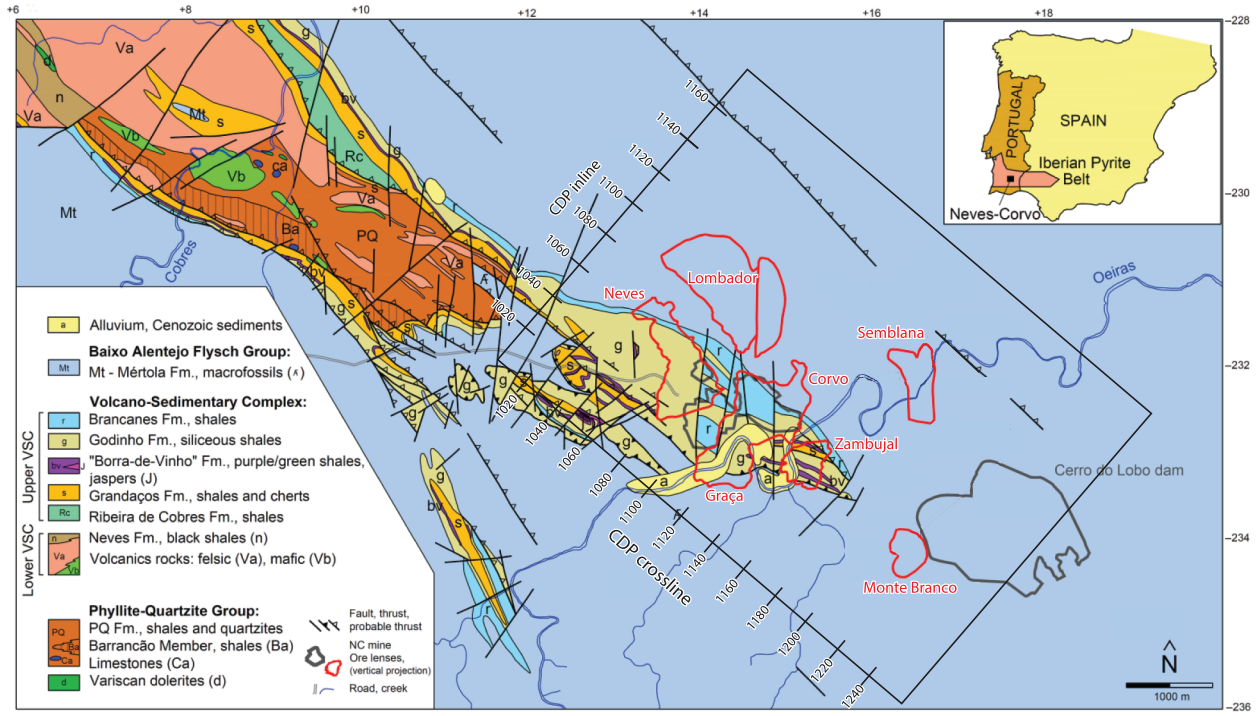

FIGURE 2 Simplified geology of the Neves-Corvo area, showing the major deposits and the 2011 3D survey area (adapted from Pereira et al., 2021).

VMS deposits have been presented by Bohlen et al. (2003), Malehmir and Bellefleur (2009) and Markovic et al. (2022).

The reprocessing results benefited from a more robust refraction static solution, improved velocity model obtained from previous research done in the mine tunnels (Donoso et al., 2021) as well as a thorough analysis of the common depth-point binning size, which is deemed essential in obtaining an improved 3D seismic volume of the study area. The study also highlights the importance of 3D seismic methods for accurate targeting and mapping by comparing them with previous 2D seismic processing results (Donoso et al., 2020).

The northern part of the 3D grid coincides with a 2019 surface and in-mine seismic survey (Figure 1), where two profiles were acquired on the surface above the Lombador deposit, while simultaneously four seismic profiles were deployed and recorded inside mining and exploration tunnels at 650 m depth, arguably the first time a seismic acquisition survey of this size has been carried out inside an active mine (Brodic et al., 2021; Donoso et al., 2021). The 3D data processing job in this article benefited from the experience and velocity models found in the 2019 survey.

GEOLOGICAL SETTING

The Neves-Corvo volcanogenic massive sulphides (VMS) deposits, located in the south of Portugal, are considered to be the richest mineralized bodies in the mineral-endowed Iberian Pyrite Belt (IPB). The IPB stretches from Spain to Portugal (Figure 2), and Neves-Corvo itself is the largest and one of the most important VMS deposits in the world (Relvas et al., 2002). The VMS at Neves-Corvo generally have thicknesses of 20–100 m that can reach up to 140 m (Oliveira et al., 2013), typically occurring as massive sulphide lenses hosting base metals (copper, zinc, tin and lead) but also sometimes as stockwork deposits. Until now, seven major lenses have been discovered in the area: Neves, Corvo, Graça, Zambujal, Lombador, Semblana, and Monte Branco (Figures 1 and 2), all located at depths ranging from 200 to 1300 m (Carvalho et al., 2021). The dominant minerals are pyrite (making them massive), chalcopyrite, sphalerite, galena and cassiterite in a lesser amount (West & Penney, 2017).

The lithostratigraphic sequence of the Neves-Corvo mine area is comprised of three main regional units (Figure 2), which are, from the bottom up: Phyllite–Quartzite Group, the Volcano-Sedimentary Complex (VSC), and the Mértola Formation (the lower unit of the Baixo Alentejo Flysch Group) (Mendes et al., 2018; Oliveira et al., 2013; Pereira et al., 2008). The VSC is divided into a Lower VSC and an Upper VSC sequence; the top of Lower VSC is of particular interest since it is where massive sulphide mineralization is found.

The Lower VSC sequence comprises essentially felsic volcanic rocks, including coherent and abundant autoclastic rhyolites and rhyodacites, pumice breccias, and minor basalt lava flows and intrusive mafic volcanic rocks with a total thickness of up to 100 m, Famennian age dark-grey shales of

13652478, 0, Downloaded from https://onlinelibrary.wiley.com/doi/10.1111/1365-2478.13269 by Cochrane Portugal, Wiley Online Library on [14/12/2022]. See the Terms and Conditions (https://onlinelibrary.wiley.com/terms-and-conditions) on Wiley Online Library for rules of use; OA articles are governed by the applicable Creative Commons License

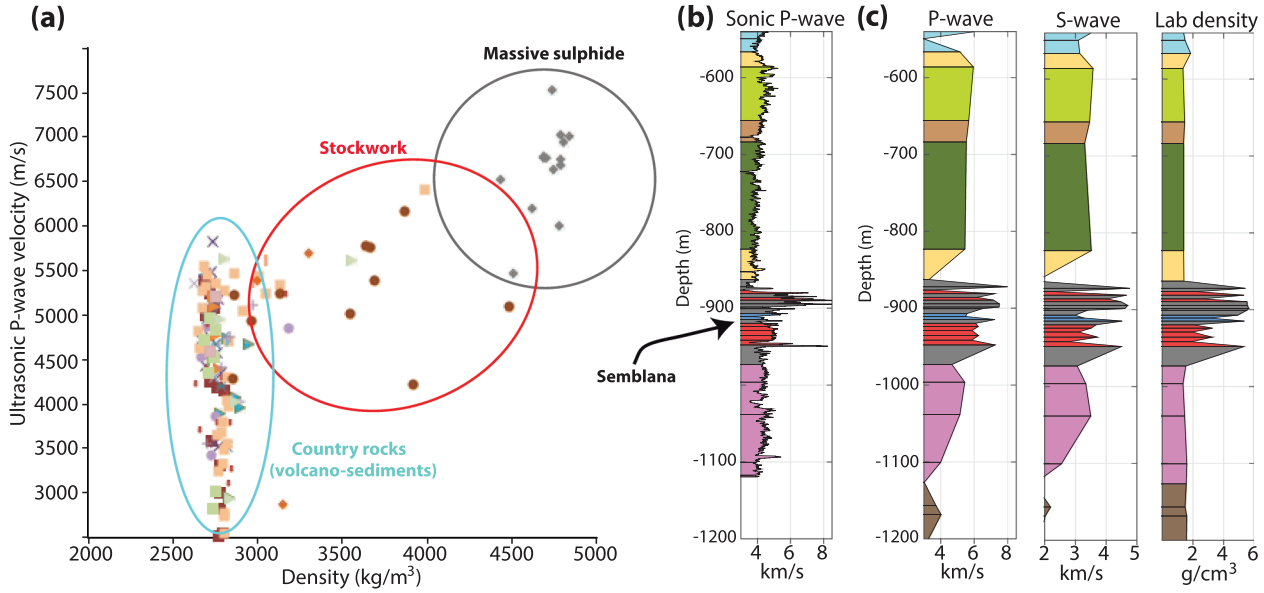

FIGURE 3 (a) Cross-plot of P-wave velocities measured at ultrasonic frequencies and laboratory-measured densities for a selection of core samples from the Neves-Corvo mining area. VMS deposits (circled in grey) show a much higher contrast with their surrounding host rock (circled in cyan) and should generate a strong seismic signal. (b) Example downhole sonic logging measurements versus core sample (c) ultrasonic P-wave and S-wave velocities and density measurements intersecting the Semblana deposit. Both downhole logging and ultrasonic measurements suggest elevated velocity and density at the Semblana deposit (adapted from Donoso et al., 2020).

approximately 40 m thick corresponding to the Corvo Formation and black pyritic shales of the Neves Formation, which vary in thicknesses from a few metres up to approximately 100 m, with interbedded massive sulphides. The Neves Formation shales are dated as being of late Famennian (Strunian) age based on fossil dating, corresponding to an age between 359 Ma (Devonian–Carboniferous boundary) and approximately 360.5 Ma (Streel et al., 2006; Streel, 2009). The Upper VSC sequence, with an approximate total thickness of 350–400 m, is composed of siliceous shales, volcanogenic sedimentary rocks and grey and black pyritic shales with minor greywackes (Oliveira et al., 2004, 2013; Pereira et al., 2008). The VSC is overlain by the Mértola Formation, the lowermost unit of the Baixo Alentejo Flysch Group (of the middle–late Visean age), a turbidite sequence comprised of alternating dark-grey shales and greywackes that can reach a thickness up to 3000 m.

After the discovery of Semblana in 2010 and Monte Branco in 2012 the area proved to be still highly prospective, with the expectation that more lenses can be found in the area and at depth, requiring more deep probing exploration methods. Seismic methods were once again selected as one of the primary methods of choice, together with gravimetric and electromagnetic methods.

The legacy 1996 data, the new tunnel-surface 2019 survey and the 2011 3D dataset studied in this work illuminate the zinc-rich Lombador deposit (ca. 150 Mt). Lombador was discovered in 1988 following an unexplained gravity anomaly (ca. 0.2 mGal), located at approximately 600–800 m depth. Lombador dips to the NE and is known to extend down to at least 1000 m depth and striking (lateral dimension) 1200 m. Semblana is a VMS deposit located at 820 m depth with up to 100 m thickness, mostly horizontal and gently dipping northeast. It includes sulphidic copper mineralization (Yavuz et al., 2015), originally discovered after revisiting legacy gravimetric data in 2009 and fully defined in 2011 following the interpretation of the 3D seismic dataset (West & Penney, 2017).

PHYSICAL ROCK PROPERTIES

Data from a 2012 rock properties study from the Neves-Corvo area comprising 164 drill core samples were made available as well as data from short-length sonic downhole logging from a few boreholes that cored through host rock and mineralization of Semblana (West & Penney, 2017; Yavuz et al., 2015). Sonic downhole logging measurements are preferred since they are closer in frequency (ca. 20 KHz) to the seismic data than the ultrasonic measurements (ca. 0.5–1 MHz). An example of physical properties, namely velocity and density from ultrasonic and downhole logging measurements, is shown from the Semblana deposit (Figure 3). A crossplot of density against P-wave velocity for core samples measured in the laboratory (ultrasonic frequency) is also presented (Figure 3a), justifying why seismic methods can be useful in not only delineating massive sulphides but also rich stockworks as they show distinctly higher densities than all types of lithologies intersected

13652478, 0, Downloaded from https://onlinelibrary.wiley.com/doi/10.1111/1365-2478.13269 by Cochrane Portugal, Wiley Online Library on [14/12/2022]. See the Terms and Conditions (https://onlinelibrary.wiley.com/terms-and-conditions) on Wiley Online Library for rules of use; OA articles are governed by the applicable Creative Commons License

TABLE 1 Main acquisition parameters for Neves-Corvo 2011

Survey parameters	
Acquisition dates	March–June 2011
Inline - crossline	Orthogonal
Receiver and source parameters	
Source	Vibroseis and impact source
Patches used for recording	28
Receiver lines per patch	11
Source lines per patch	10
Receiver line distance	90 m
Source line distance	90 m
Receiver line length (per patch)	1605 m
Source line length (per patch)	1620 m
Receiver interval	15 m
Source interval	45 m
Receiver density	634 geophones per km^2
Source density	368 source points per km^2
Live channels per shot	1188
Recording parameters	
Record length	2000 ms
Sampling rate	2 ms
Total number of traces	~ 7800000

in the borehole. Interestingly, both downhole logging and ultrasonic velocities show generally decreasing trends with depth and, as expected, the ultrasonic velocities show much higher velocities than the sonic ones (Salisbury et al., 2003). A closer look at the velocity information gives an average host rock velocity of approximately 4300 m/s and a much higher one for the massive sulphides, up to 5500–6000 m/s in the sonic logging data.

It is evident from the plotted data that massive sulphides and stockwork mineralization have higher velocities (both for P- and S-waves) and density than their surrounding host rock (hanging and footwall). This observation supports the idea that massive sulphides are capable of producing strong seismic reflections, detectable if the deposit geometry and thickness allow for adequate signal-to-noise ratio for their imaging (e.g., Malehmir et al., 2012; Salisbury et al., 2000, 2003; Yavuz et al., 2015).

THREE-DIMENSIONAL SURFACE SEISMIC DATASET

The 3D surface reflection seismic survey was conducted by Somincor (a Portuguese subsidiary of Lundin Mining Corporation) through a service company from March to June 2011.

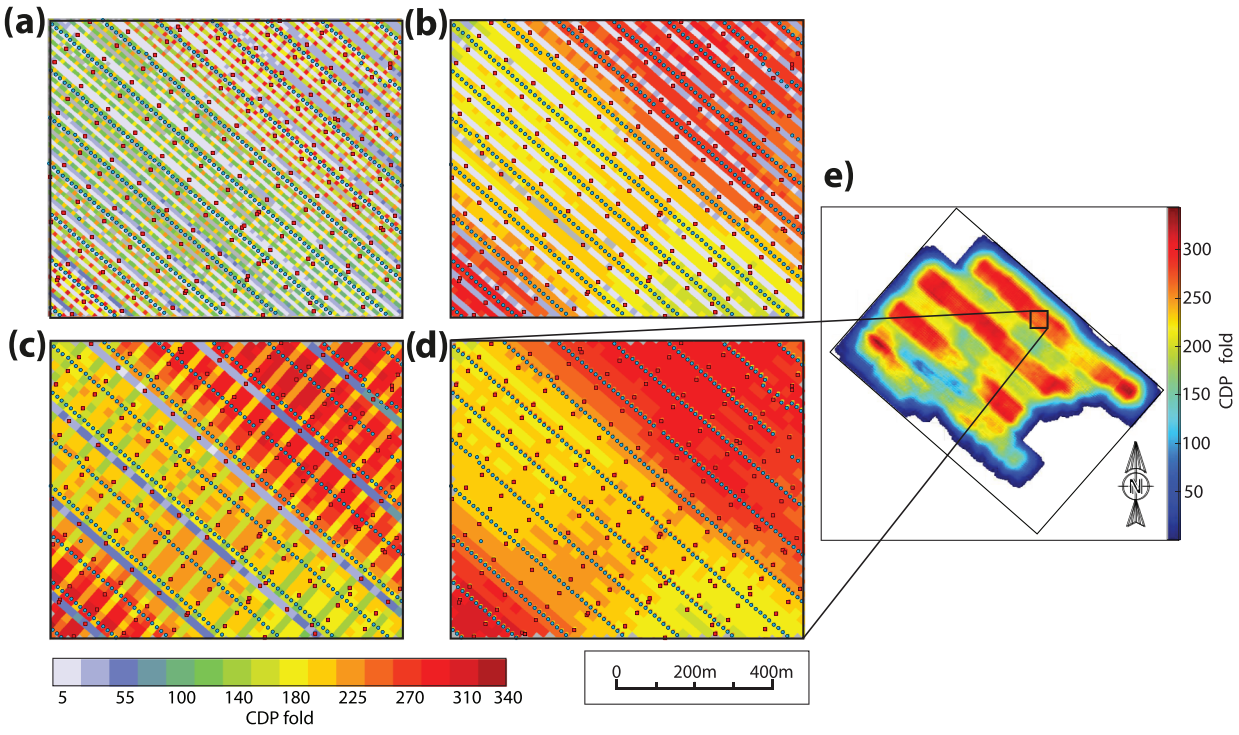

FIGURE 4 CDP fold coverage over the Semblana using different CDP binning sizes. (a) 10 m × 10 m, (b) 15 m × 15 m, (c) 20 m × 20 m, and (d) 22.5 m × 22.5 m. (e) Full CDP fold coverage for 22.5 m × 22.5 m bin sizes, lower acquisition footprint, and improved fold coverage are found. Small red squares are shot positions, and small blue circles are receiver positions. All four cases shown belong to the same small area on the fold coverage map and have an identical scale.

13652478, 0, Downloaded from https://onlinelibrary.wiley.com/doi/10.1111/1365-2478.13269 by Cochrane Portugal, Wiley Online Library on [14/12/2022]. See the Terms and Conditions (https://onlinelibrary.wiley.com/terms-and-conditions) on Wiley Online Library for rules of use; OA articles are governed by the applicable Creative Commons License

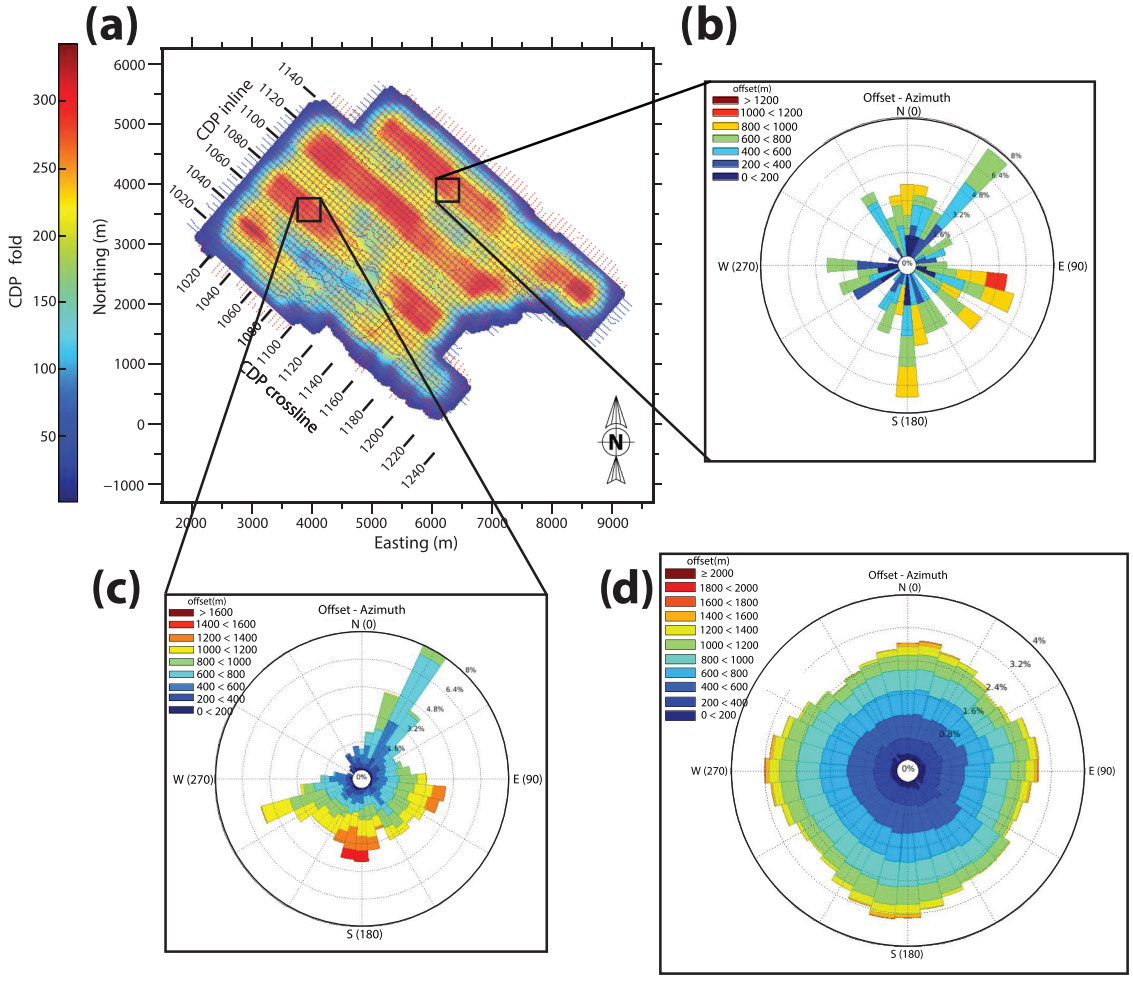

FIGURE 5 (a) 3D Acquisition geometry projected onto the CDP fold coverage for the 22.5 m × 22.5 m binning size that was used for the processing of the dataset. (b) Rose diagram of azimuth distribution for bins illuminating (b) Semblana and (c) Lombador. (d) Azimuth distribution for the entire 3D dataset shows a more uniform offset-azimuth distribution.

The 3D grid covered an area of approximately 6 km (NW-SE) by 4 km (NE-SW); the receiver lines were orthogonal to the source lines forming a rather orthogonal acquisition geometry, resulting in nearly eight million seismic traces over an area of 24 km^2. Due to access issues in some areas, particularly the mine tailing area in the southeast corner of the 3D grid, no receivers were positioned and only sources were activated. The main seismic data acquisition parameters of the 3D dataset are summarized in Table 1. Most of the survey was completed with a 138 kN (31,022 ft-lb) Mertz M22-601 Vibroseis and using a sweep frequency range of 10–120 Hz. A few patches near the Lombador village were done with a 16-kJ (11,800 ft-lb) Hydrapulse accelerated weight drop system (West & Penney, 2017).

The 3D data from 2011 were made available for this study as raw cross-correlated shot gathers in SEG-Y format, which included some first break picks stored in the trace headers from the initial data processing works. No support information nor written field reports were made available, most of the acquisition parameters, when unavailable in the trace headers, were extracted from earlier publications from this 3D dataset, such as West and Penney (2017) and Yavuz et al. (2015).

In terms of data quality, the Neves-Corvo 3D data show a mixed signal-to-noise ratio (S/N), some recording patches are rather poor, in particular for far offsets. Others show good S/N implying that ambient noise and surface conditions differ significantly in the Neves-Corvo, which further justifies a good static solution and tailored-processing workflow for successful imaging of its subsurface structures.

DATA PROCESSING

A conventional pre-stack seismic data processing sequence was implemented focusing on attenuating noise such as surface waves and ambient noise, while post-stack steps were tested and used in order to enhance reflections, leading up to dip move-out (DMO) corrections, F_{XY}-deconvolution and

13652478, 0, Downloaded from https://onlinelibrary.wiley.com/doi/10.1111/1365-2478.13269 by Cochrane Portugal, Wiley Online Library on [14/12/2022]. See the Terms and Conditions (https://onlinelibrary.wiley.com/terms-and-conditions) on Wiley Online Library for rules of use; OA articles are governed by the applicable Creative Commons License

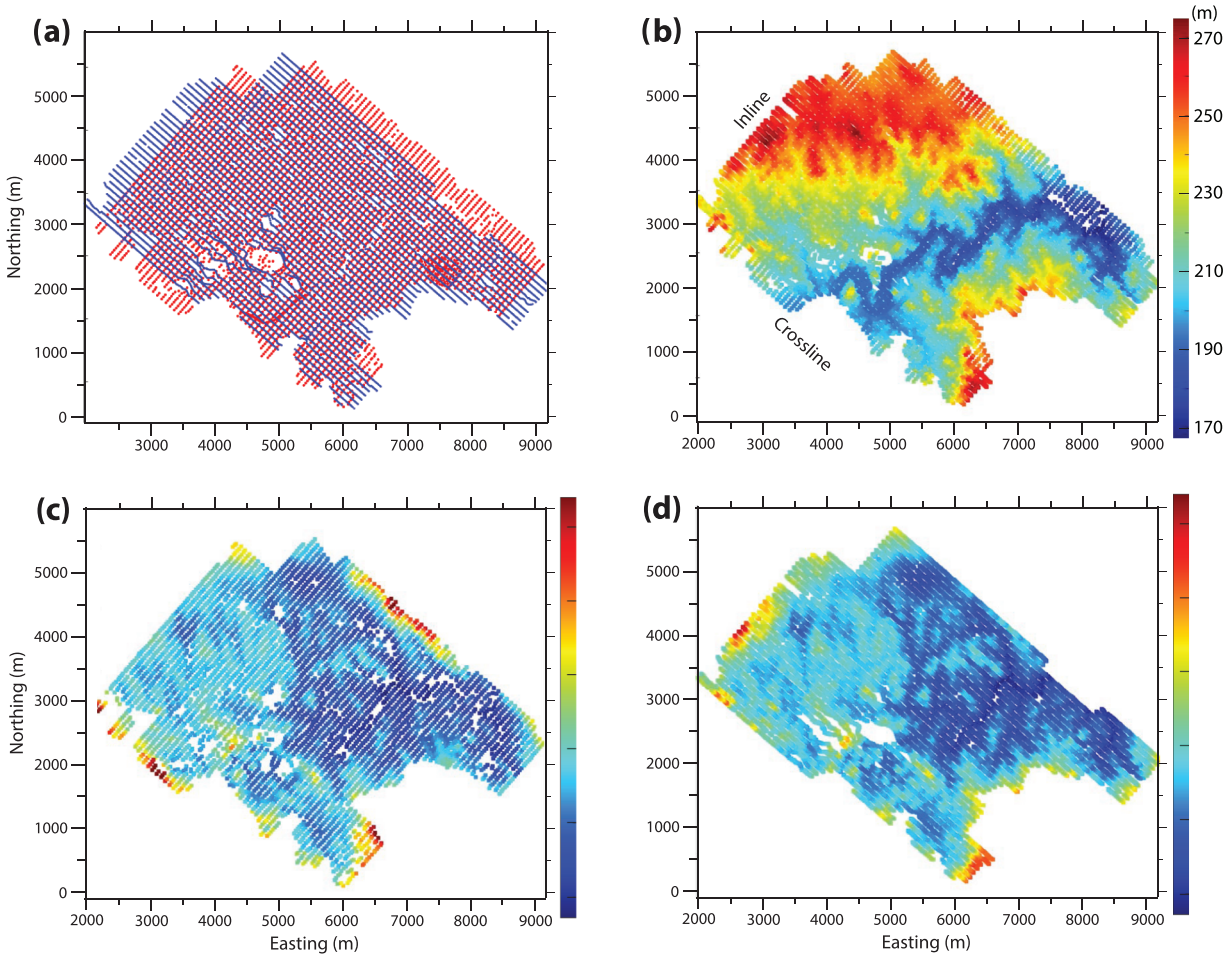

FIGURE 6 (a) Source and receiver positions (dense red and blue points, respectively). (b) Topography map of the study area. Source (c) and (d) refraction static corrections estimated for the 3D survey.

post-stack migration. Every processing tool and parameter was tested not only in the shot gather domain but also by stacking the data and comparing the processing effects on the reflections continuity before and after every step, in order to guarantee a continuous improvement in the imaging results.

Common depth-point binning and pre-processing

Defining an adequate common depth-point (CDP) binning size is one of the first processing steps of any 3D seismic dataset. In fact, bins are carefully selected even during the planning and acquisition steps so that targets are properly imaged with high fold and resolution, also considering a uniform offset and azimuthal coverage for each CDP bin (Cordsen et al., 2000; Vermeer, 1998). As shown in Cheraghi et al. (2013), ignoring a thorough study of the bin and its effect would lead not only to aliased data but also severe acquisition footprints, which is a more significant issue for hard-rock seismic data than for sedimentary settings. It is, for example, much more straightforward to perform trace interpolation for data from sedimentary basins than those of hard-rock data that present short lateral continuation for reflections. To select an appropriate 3D binning size, the desired vertical resolution of the target must be considered, in the presence of a dipping reflector, since there is a relationship between the expected vertical resolution and the horizontal resolution. An equation (Yilmaz, 2001) that relates the bin size in a given direction, frequency and subsurface dip is defined as

$$\text{Bin size} \leq \frac{V_{RMS}}{4 f_{\max \sin \theta}}, \tag{1}$$

where V_{RMS} is the root-mean square (RMS) velocity at the zone of interest and θ the dip angle, $f_{\max}$ is the maximum frequency at the target seismic reflection to be retained or non-aliased. With an average RMS velocity of 4500 m/s and the maximal useful frequency of the reflector being 70 Hz, with a dipping angle of approximately 45°, the calculated bin size to prevent frequencies aliasing below 80 Hz should be approximately 20 m. After obtaining an appropriate

13652478, 0, Downloaded from https://onlinelibrary.wiley.com/doi/10.1111/1365-2478.13269 by Cochrane Portugal, Wiley Online Library on [14/12/2022]. See the Terms and Conditions (https://onlinelibrary.wiley.com/terms-and-conditions) on Wiley Online Library for rules of use; OA articles are governed by the applicable Creative Commons License

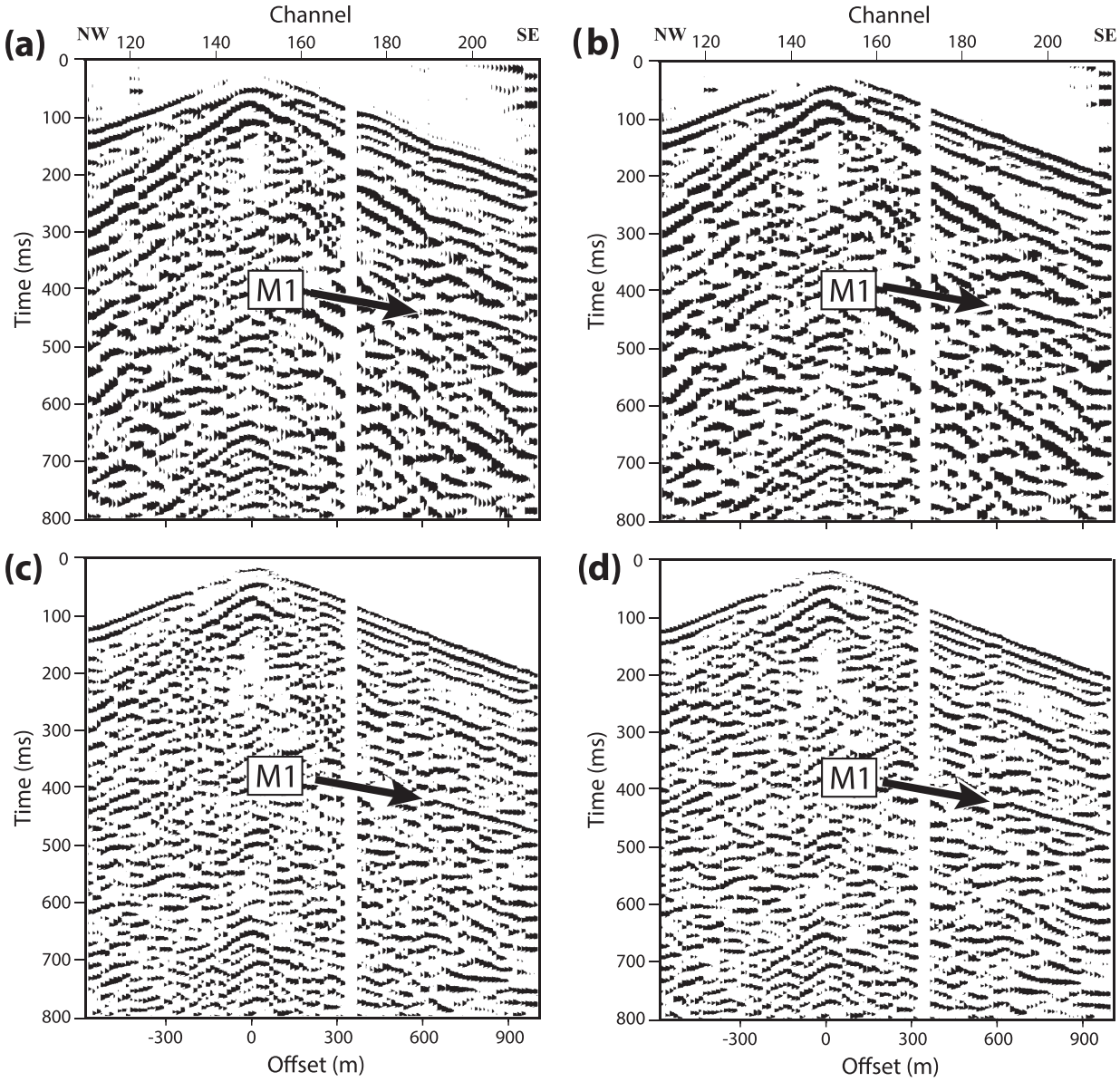

FIGURE 7 Close-up of a raw shot gather from one receiver line showing data quality and improvement in S/N after some processing steps (a) raw data, (b) elevation and refraction statics, (c) band-pass filter and spectral equalization, (d) F-k filter. Note the increase in coherency for reflection (M1) shown with black arrows. Automatic gain control has been applied for display purposes.

theoretical estimation for the bin size, different-sized CDP binning grids were designed and tested on the data itself namely: 10 m × 10 m, 15 m × 15 m, 20 m × 20 m and 22.5 m × 22.5 m (Figure 4). Only when a 22.5 m × 22.5 m bin size is used the fold coverage becomes more uniform and no zero-fold coverage appears (Figure 4d), reinforcing the importance of properly choosing the CDP binning size during the first stages of data preparation.

Once the appropriate binning size was chosen, the data pre-processing work continued by visually inspecting approximately 14000 shot gathers that comprise the dataset, finding and deleting void gathers, while at the same time removing noisy and dead traces. Approximately 200 noisy shot gathers were removed, in particular, some at far offsets.

The raw shot gathers had first-break arrivals saved in the headers, but upon visual inspection it was found that most of these were not consistent with the reality of the data, so a MATLAB code was developed and implemented to find and remove the first-break values that were not consistent with the known offset values. Also a great deal of time was spent manually repicking where necessary. The corrected first breaks provide improved imaging results through surface-consistent refraction static corrections, which is a key step for nearly all hard-rock datasets (Malehmir et al., 2012).

13652478, 0, Downloaded from https://onlinelibrary.wiley.com/doi/10.1111/1365-2478.13269 by Cochrane Portugal, Wiley Online Library on [14/12/2022]. See the Terms and Conditions (https://onlinelibrary.wiley.com/terms-and-conditions) on Wiley Online Library for rules of use; OA articles are governed by the applicable Creative Commons License

As part of the data pre-processing analysis, azimuth distribution of the dataset was studied and plotted as a rose diagram (Figure 5) for areas of interest (Figure 5b,c) and for the entire dataset (Figure 5d). For the whole dataset, the offset-azimuth distribution is quite uniform (Figure 5d) although this should be looked at with care; a closer look at bins in the Lombador area (Figure 5c) shows a lack of long offsets in the north-west direction, whereas for Semblana (Figure 5b) it suffers from an irregular azimuthal illumination.

Pre-stack signal enhancement

After the pre-processing steps, a model for refraction static corrections was calculated from the corrected first break values (Figure 6), resulting in a much-improved continuity of reflections on the shot gathers. Some additional tools applied for attenuating noise on the shot gathers were spectral equalization and top-mute application; the latter was done by removing the direct wave by deleting a few milliseconds below the first break picks where available. A linear velocity filter was also used at 2200 m/s to remove strong surface waves as well as F-k filtering. After the abovementioned processing steps, strong reflections associated with Lombador (M1 in Figure 7) and Semblana deposits could be identified in the shot gathers.

Velocity analysis

Constant velocity stack (CVS) panels were generated and visualized along inline and crossline directions to inspect potential reflections and their velocity sensitivity and help define an initial brute normal-moveout (NMO) velocity model, finding a homogeneous velocity field with an average of approximately 5400 m/s. This was followed by iterative velocity picking and stacking that guaranteed the best imaging results for the reflections observed, with two major ones of particular interest. The first is on the eastern side of the survey, mostly flat and continuous with a stacking velocity of 5200 m/s; the second is on the northeast of the survey area, steeply dipping with an angle of approximately 45° and a stacking velocity of 6500 m/s. The former is likely associated with the Semblana, and the latter is associated with the Lombador deposit. It is worth noting that high stacking velocity values at this stage of processing may only be associated with dip-dependent stacking velocities and not necessarily the presence of high-velocity rocks.

Additional steps were used on the stacked data to provide reflection coherence enhancement, some of which were F_{XY}-deconvolution and low-frequency noise removal. The NMO-corrected unmigrated stacked volume (Figure 8a) presents not only strong reflections associated with the known Lombador

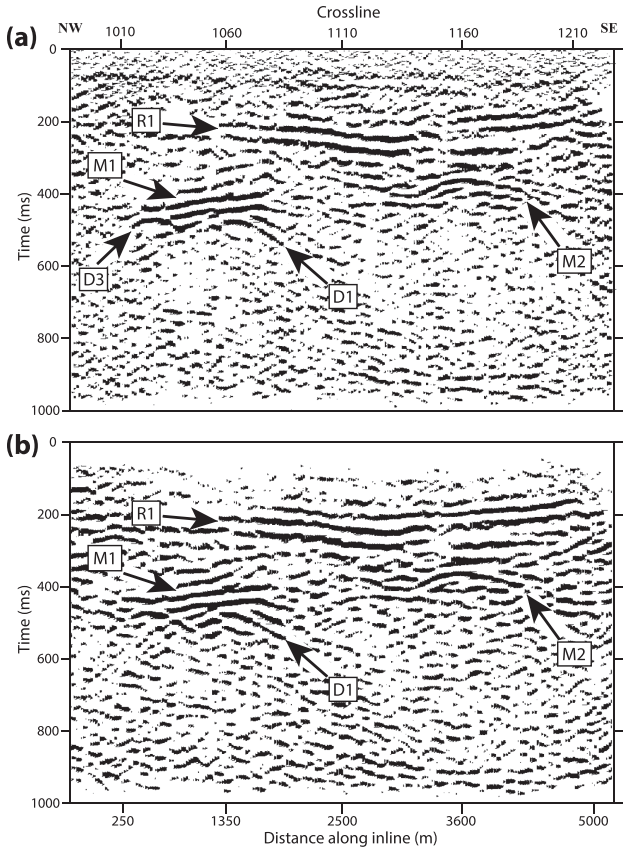

FIGURE 8 An inline (1118) extracted from the unmigrated stacked cube (Figure 1). (a) NMO corrected only the unmigrated stack and (b) NMO and DMO corrected the unmigrated stack. Note reflections associated with the Lombador (M1) and Semblana (M2) deposits, and two diffraction patterns (D1 and D3) adjacent to the Lombador deposit. The shallower flat-lying reflection (R1) is from the Upper Flysch group contact lithology.

(M1 in Figure 8) and Semblana (M2 in Figure 8) but also strong hyperbolic features (D1 and D3 in Figure 8a), which are likely diffraction possibly originated by the edges of the deposits.

Dip move-out stack and migration

When correcting the CDP gathers using an NMO velocity, it is assumed that the subsurface is comprised of horizontal layers but in reality the NMO velocity needed for dipping reflections (V_{dip}) are not true velocities (V) in the sense that they have to compensate for the dip angle of the reflector (α) in order to properly stack, more specifically the cosine of the dipping angle ($\cos\alpha$), as indicated by the following relation:

$$V_{\text{dip}} = \frac{V}{\cos\alpha}. \quad (2)$$

13652478, 0, Downloaded from https://onlinelibrary.wiley.com/doi/10.1111/1365-2478.13269 by Cochrane Portugal, Wiley Online Library on [14/12/2022]. See the Terms and Conditions (https://onlinelibrary.wiley.com/terms-and-conditions) on Wiley Online Library for rules of use; OA articles are governed by the applicable Creative Commons License

TABLE 2 Main processing steps applied to the Neves-Corvo 3D dataset, 2021

Process	Parameter
Data input	SEG-Y data input
Geometry assignment	From trace headers and field reports
Common depth-point (CDP) binning	CDP size 22.5 m × 22.5 m
Trace editing	Kill noisy traces
First break picking	Automatic and manual
Refraction static correction	Two-layer model and using first breaks
Trace muting	Top mute using first breaks
Band-pass filter	5–20–80–100 Hz
Spectral equalization	Filter 5–20–80–100 Hz
Air blast attenuation	Attenuation for velocity: 330 m/s
Linear move-out correction	Velocity: 4850 m/s
Top-mute	Linear moveout based for removing direct wave
Linear velocity filter	Attenuation for velocity: 2200 m/s
Automatic gain control	Window: 250 ms
3D dip move-out	Maximum offset: 2000 m
Velocity analysis	Constant velocity stack panels, iterative
Normal-moveout corrections	30% stretch mute
FK-mute	Surgical muting
Surface-consistent residual statics	Twice and iterative
Stack	Unity
F_{XY}-deconvolution	Window length: 100 ms
Low-pass filter	130–150 Hz
Migration	Phase-shift: 1D velocity model
Time-to-depth conversion	1D velocity, average 5100 m/s

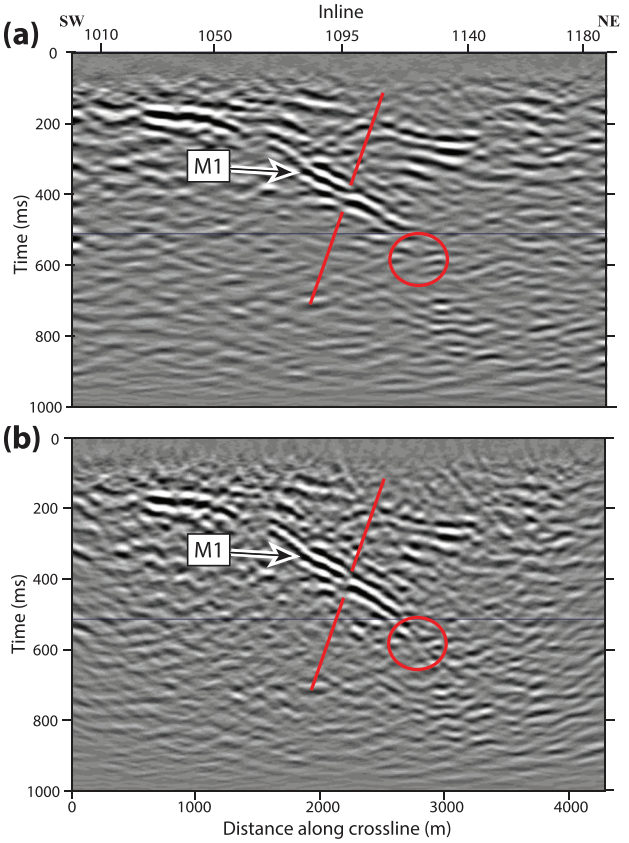

FIGURE 9 A crossline (1070) extracted from the migrated seismic volume. (a) Finite-difference migrated and (b) Phase-shift migrated. Phase-shift migration better preserves the Lombador (M1) reflection and a possible fault (indicated by red lines) and edge features (circled in red). The finite-difference migration shows smoother reflections and lower resolution.

To remove the dip–velocity dependency and better position the actual reflection position in the subsurface, the DMO correction is needed. This becomes more important when reflections crosscut each other with different angles, hence conflicting dips, meaning that at an intersection only one velocity can be used for stacking (Deregowski, 1986). In this study a 3D DMO process was applied, calculated using 40 panels every 50 m, for a maximum offset of 2000 m.

Once the DMO corrections were applied to the gathers a new dip-independent stacking velocity model was generated, the same as before by comparing CVS panels, to obtain the best continuity and imaging of the features of interest. The new velocity model for the DMO-corrected gathers is more homogeneous than the one found for the conventional stacking, no extreme high velocities were needed to properly image the highly dipping Lombador, reflections are more continuous and diffraction signals partially collapsed (Figure 8b). The relevant processing steps applied to the Neves-Corvo 3D seismic data are summarized in Table 2.

Various post-stack migration methods were tested (e.g., Kirchhoff, Stolt, phase-shift and finite-difference). For selecting the final migration method, particular testing was done with finite-difference (Figure 9a) and phase shift (Figure 9b) migration algorithms because these generated fewer artefacts. The phase-shift migration algorithm was finally selected since it better preserved a speculated fracture crossing the Lombador deposit and provided a better definition of its geometry (Figure 9b). A one-dimensional (1D) migration velocity model was available for the same area of interest from previous work by Donoso et al. (2021); this velocity was used for the final migration results.

Time-to-depth conversion is needed for proper 3D depth visualization and correlation with known geology. A 1D velocity model, with an average value of 5100 m/s, based on data from a 2019 surface-tunnel seismic experiment conducted in the same area and reported by Donoso et al. (2021), was used. The obtained migrated seismic images were

13652478, 0, Downloaded from https://onlinelibrary.wiley.com/doi/10.1111/1365-2478.13269 by Cochrane Portugal, Wiley Online Library on [14/12/2022]. See the Terms and Conditions (https://onlinelibrary.wiley.com/terms-and-conditions) on Wiley Online Library for rules of use; OA articles are governed by the applicable Creative Commons License

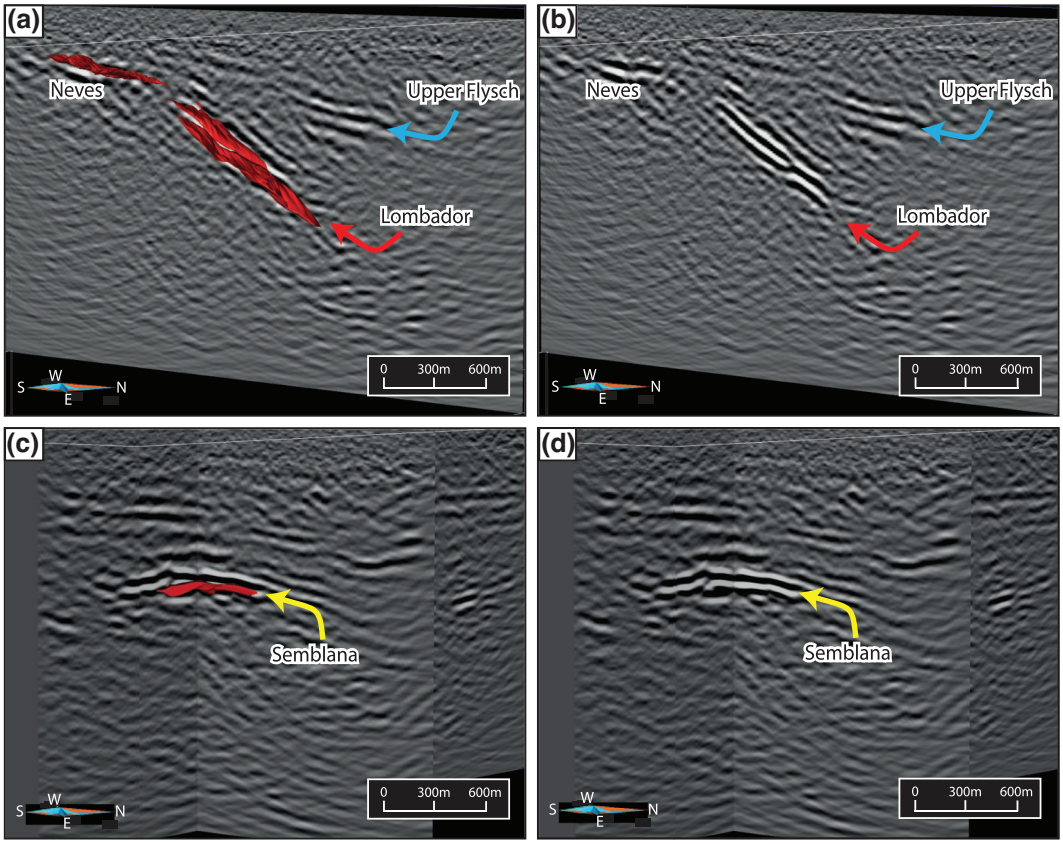

FIGURE 10 Selected 3D views from a number of inlines and crosslines of the migrated volume visualized with deposit surfaces. (a) East view of crossline 1070 intersecting the known Lombador deposit surface (red). (b) East view of the same crossline without the Lombador surface. (c) East view of inline 1118 and crossline 1145 intersection with the Semblana deposit surface (red). (d) East view of the same inline 1118 and crossline 1145 intersection without the Semblana surface. The vertical scale is equal to the horizontal scale.

compared with the known drill-hole constrained 3D surface models of the Lombador and Semblana deposits (Figure 10) and used as markers to judge if the velocity profile was accurate enough, or if adjustments were needed to match with the known surfaces of these deposits. The known surfaces of Lombador and Semblana (red surfaces in Figure 10a,c) when compared with the 3D seismic imaging results from the current article display a consistent match, both in shape and depth. This is a validation of the velocity model chosen for the time-to-depth conversion. A fracture zone that crosses Lombador (Figures 9b and 10b) can be observed in the seismic data, showing great resolution at depth.

RESULTS AND DISCUSSION

Common depth-point binning

During the first stages of the processing work, the CDP binning size was first calculated theoretically using equation (1) and afterwards validated empirically by testing several binning sizes (Figure 4). These choices were justified based on receiver and shot spacing assuming that a 2D binning criteria could also serve the purpose and given the smaller size of the bins, leading to a higher resolution seismic volume while fold would be lower for smaller bins. With 10 m × 10 m bins (Figure 4a), most of the created bins and inlines show no fold coverage, while using 15 m × 15 m bins acquisition footprint manifested in the fold coverage becomes quite strong (Figure 4b). Although 20 m × 20 m bins show a better and more uniform fold coverage, given the acquisition setup of the Neves-Corvo, it leaves some inlines with nearly zero-fold (Figure 4c). Ultimately and nearly only when a 22.5 m × 22.5 m bin size was used the fold coverage became more uniform and no inlines with zero-fold coverage appeared (Figure 4d) and reflections started to be observed in the stacked volume. The 22.5-m bin size may be large for this survey; however, it allows to delineate reasonable larger size volcanogenic massive sulphides (VMS) deposits. CDP binning is often overlooked as a perfunctory step, but in this case it is shown how a small difference of even 2.5 m (between Figure 4c,d) can accumulate every inline until zero-fold inlines appear. Thus, we highlight the importance of careful bin size study during the reflection data processing and more importantly during the data acquisition. The Neves-Corvo 3D dataset although large in area, with a 22.5-m bin

13652478, 0, Downloaded from https://onlinelibrary.wiley.com/doi/10.1111/1365-2478.13269 by Cochrane Portugal, Wiley Online Library on [14/12/2022]. See the Terms and Conditions (https://onlinelibrary.wiley.com/terms-and-conditions) on Wiley Online Library for rules of use; OA articles are governed by the applicable Creative Commons License

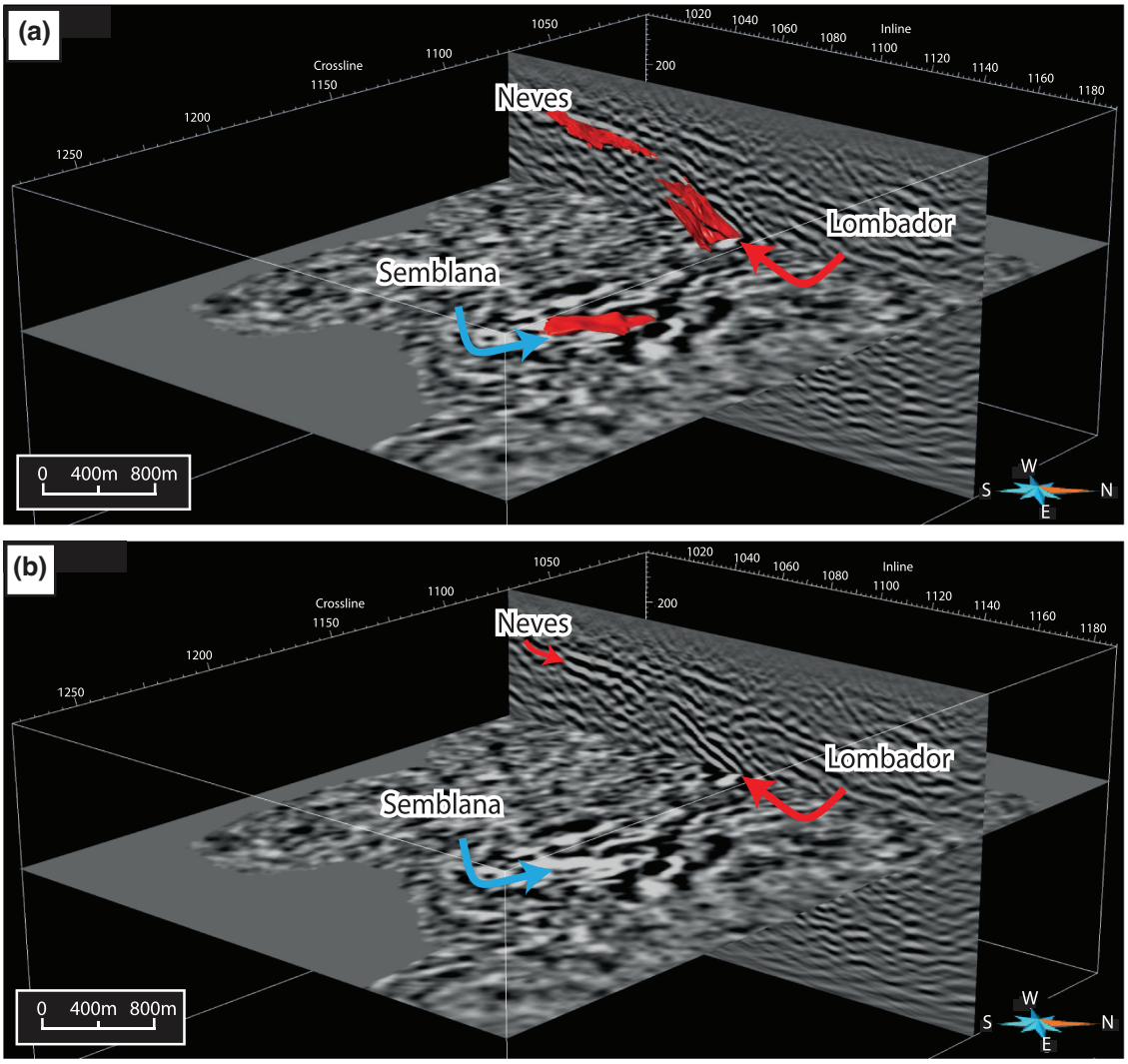

FIGURE 11 3D view of the migrated volume with Neves and Lombador (red arrows), and Semblana (blue arrows) surfaces. (a) 3D view intersecting the known deposit surfaces and (b) the same 3D view without the deposit surfaces.

size, can be considered medium sized in terms of resolution compared to those conducted using much higher folds and CDP bin sizes of 10–15 m such as in Canada, Finland and Sweden.

Three-dimensional versus two-dimensional data

Established methodology in mineral exploration has relied mostly on potential field and electromagnetic methods for detecting anomalies, later drilled for direct detection. Seismic methods are less frequently employed due to a perceived higher cost. When seismic is used, it is mostly for the acquisition of 2D profiles rather than 3D seismic (Malehmir et al., 2017). A common practice in seismic exploration for both hydrocarbon and mineral exploration is to first use long offset (usually low resolution) 2D profiles for detecting areas of interest and testing surveying parameters. This is then followed by a more specific targeted survey, usually a 2D seismic survey and in a few particular cases a 3D survey and/or VSP (e.g., Bellefleur et al., 2004). It is possible, in certain cases, that implementing a full 3D seismic survey from the start could represent significant savings in time and cost. This becomes even more relevant when a dedicated 2D seismic survey cannot fully identify the dip and extent of a geological structure of interest due to the geometrical properties of wave propagation.

A depth-slice visualization of the Neves-Corvo 3D seismic cube offers a better view of the two most dominant reflections in the Neves-Corvo volume. In particular, the shape of the Semblana deposit, derived from boreholes, shows a good correlation with the seismic amplitude response observed in the depth slice (Figure 11a). The Neves–Lombador deposits and their discontinuous character are also evident in the 3D view (Figure 11b).

13652478, 0, Downloaded from https://onlinelibrary.wiley.com/doi/10.1111/1365-2478.13269 by Cochrane Portugal, Wiley Online Library on [14/12/2022]. See the Terms and Conditions (https://onlinelibrary.wiley.com/terms-and-conditions) on Wiley Online Library for rules of use; OA articles are governed by the applicable Creative Commons License

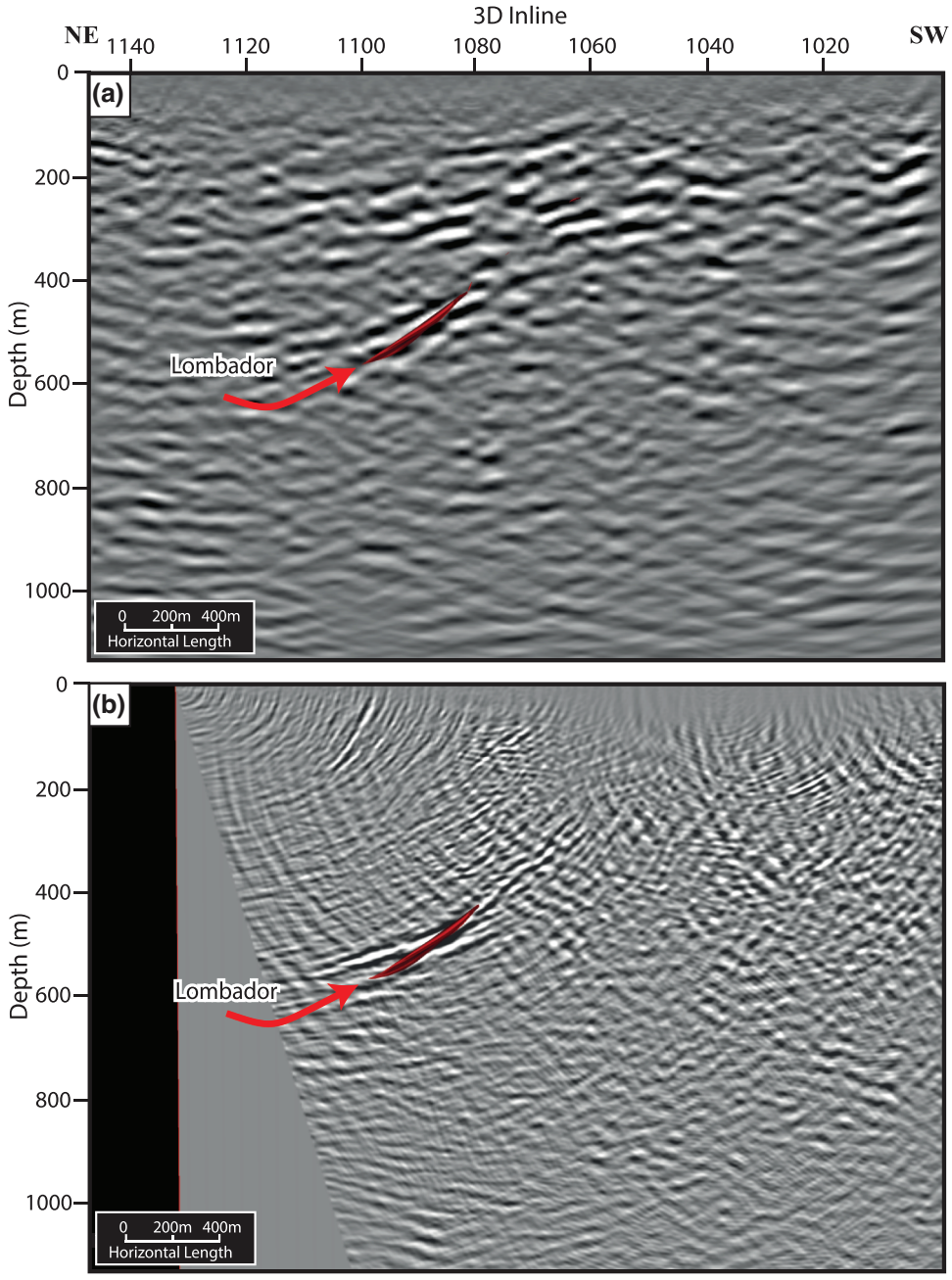

FIGURE 12 Comparison between (a) the 3D migrated volume (crossline 1030; this work) with (b) the reprocessed 2D legacy data (migrated section 96PS04; Donoso et al., 2020). Both the 3D crossline and the 2D profile intersect the Lombador deposit (red surface)

The northern part of the study area was previously investigated using reflection seismic methods: reprocessing of 2D legacy data by Donoso et al. (2020) and a new surface and tunnel 2D seismic survey (Brodic et al., 2021; Donoso et al., 2021). We emphasize why 3D data are the ultimate solution for proper resource identification and positioning in hard-rock mineral exploration. Elastic waves propagate in a 3D manner, and a 2D seismic reflection survey cannot account for this due to the intrinsic geometrical and physical limitations of imaging a 3D geological structure with 2D seismic technology, mostly since 2D fails to account for the out-of-plane components of dipping reflections (Wu et al., 1995), even after migration; resulting in what Herron & Smith (2019) refer to as structural misties in migration. Although a mistie could be small (a few to tens of milliseconds), and not apparent in the presence of low-quality data, it might also represent hundreds of metres in complex geological structures (for a VMS example in Canada, see Malehmir et al., 2017). The basic limitation of 2D migration lies in the common but invalid assumption that all dipping reflections observed on a 2D profile are true dips, where there is no actual way of determining the true components of dip that are not vertical to the plane.

13652478, 0, Downloaded from https://onlinelibrary.wiley.com/doi/10.1111/1365-2478.13269 by Cochrane Portugal, Wiley Online Library on [14/12/2022]. See the Terms and Conditions (https://onlinelibrary.wiley.com/terms-and-conditions) on Wiley Online Library for rules of use; OA articles are governed by the applicable Creative Commons License

In other words, it is impossible to distinguish between the true and apparent dips of a reflection by using only a 2D seismic profile. This was already showcased at the Neves-Corvo site by Donoso et al. (2021) via 3D exploding reflector forward modelling constructed using the true geometry of the Lombador body.

It is possible to compare the current 3D imaging work with the previous (Donoso et al., 2020) reprocessing of legacy 2D data. Figure 12 shows the migrated 2D section of profile 96PS04 (Figure 1) and the same position in depth for the 3D (crossline 1030) both intersecting the same area of the known Lombador surface. Although in both cases (2D and 3D) the main reflection matches the Lombador position in depth, the 2D reflection (Figure 12b) fails to match the Lombador down-dip angle, whereas the 3D does match the Lombador shape, depth and dip angle nearly perfectly. Also, the 2D migrated section shows a down-dip extension of the Lombador, this can be attributed to a lateral out-of-plane contribution since the 3D results have shown that this extension exists (crossline 1070 in Figures 10a,b and crossline 1070 in Figure 11) for approximately 200 m southeast and 1000 m further northwest; hence, an exploration survey based solely on 2D seismic data would have shown a false-positive result regarding the true shape of the Lombador deposit.

Edge-generated diffraction

When inspecting the 3D unmigrated stacked volume, some strong diffraction patterns (D1, D2 and D3) were identified together with the Lombador reflection (D1 and D3; Figure 8a), Studying these diffraction signals along inlines, crosslines and time slices provides an interesting insight: Lombador reflections show a dented pattern suggesting faulting. In the inlines, the strongest diffraction's apex is not entirely centred at the middle of these dented Lombador reflection, rather asymmetrically towards the southeast (Figure 8a). To provide a better understanding, the observed diffraction patterns were interpreted on the unmigrated 3D volume (Figure 13a) and compared with the known Lombador deposit surface (Figure 13b).

Diffracted waves are the result of a travelling wavefield scattered by sharp geometric or lithologic discontinuities. Seismic diffraction patterns can be categorized as point diffraction, caused by small-scale heterogeneities; and edge diffraction caused by linear-like diffractors (e.g., tunnels, edges representing termination of continuous reflectors, fault planes, and fracture zones) (Rochlin et al., 2021), following the geometric theory of diffraction (Keller, 1962; Klem-Musatov, 1994).

In the case of edge diffraction, when an incident wave propagates in the direction oblique to the edge, the diffracted wavefronts form cones with the edge as their common axis

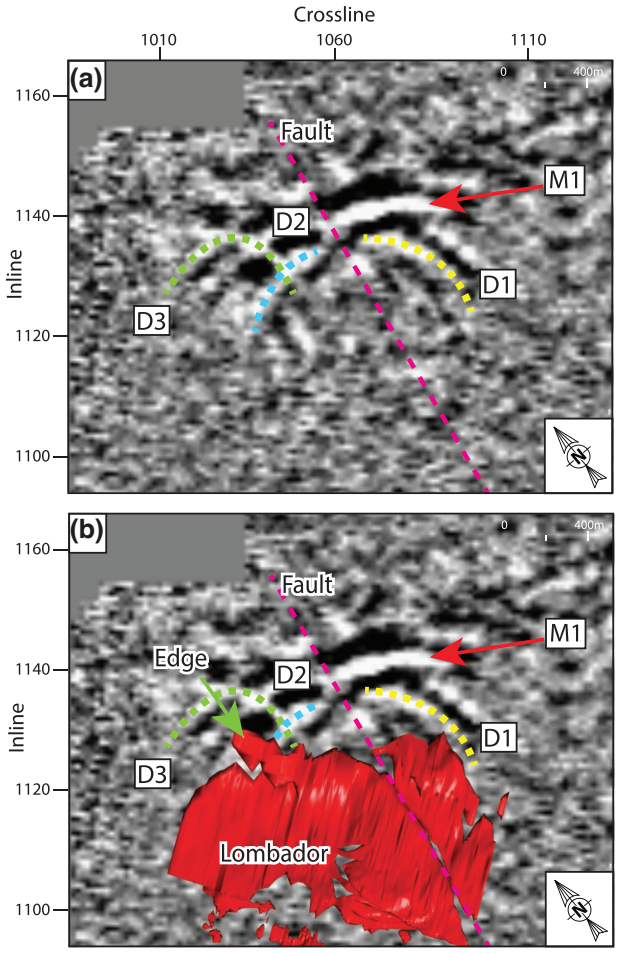

FIGURE 13 Close-up depth-slice view of reflection M1 at 620 m. (a) Interpreted diffraction patterns: D1 in yellow, D2 in cyan and D3 in green, Lombador fault in magenta. (b) Lombador deposit surface in red. Notice that the edge features of the Lombador faulting zone match D1 and D2 diffraction patterns, implying that they have originated from a faulted Lombador deposit. D3 matches the northernmost edge of Lombador.

(Keller, 1962). This cone-like projection signature from a linear diffractor is consistent with the diffraction patterns in our 3D unmigrated volume (D1 and D2 in Figure 13a), hinting that the diffraction signature observed is caused by linear edge features within the Lombador deposit. The Lombador deposit is known to be fractured from north to south (Figure 13b in magenta). Based on the observed diffraction pattern (D1 and D2) and dented character of the Lombador reflection, we argue that the Lombador is faulted with a throw of 20–30 m.

Another observed diffraction pattern (D3 in Figure 13a,b) is most likely generated by the tip and northwestern edge of the Lombador deposit, being an additional tool for detecting the lateral limits of a mineral deposit and being an example of how a diffraction pattern in theory could be used to identify structural features that might not be readily seen in a conventional low signal-to-noise ratio stacked data.

13652478, 0, Downloaded from https://onlinelibrary.wiley.com/doi/10.1111/1365-2478.13269 by Cochrane Portugal, Wiley Online Library on [14/12/2022]. See the Terms and Conditions (https://onlinelibrary.wiley.com/terms-and-conditions) on Wiley Online Library for rules of use; OA articles are governed by the applicable Creative Commons License

CONCLUSIONS

The Neves-Corvo mining area provides an example of steeply dipping volcanogenic massive sulphides (VMS) lenses in a crystalline environment that requires a dedicated selection of parameters and tools of 3D seismic data acquisition and processing to provide targeted imaging of VMS deposits of economic interest. In our processing work, three-dimensional (3D) common depth-point binning size was paramount for proper 3D imaging. We have provided a comparison between 3D seismic results and a previous two-dimensional (2D) reprocessing work illustrating how the 3D survey better images the extension of the Lombador deposit and the 2D survey provides a false-positive result for its depth extension.

It was observed how diffraction features can be useful for detecting strong edge and structural features that might not be readily visible under low signal-to-noise ratio conditions or using conventional potential-field methods. The diffraction signals observed in the Neves-Corvo 3D volume are consistent with linear edge diffraction signatures, implying they are associated with linear features such as faults, within the Lombador deposit.

We have shown how 3D seismic data acquisition and processing are instrumental for adequate VMS deposit targeting and imaging in a hard-rock environment. It would not have been possible to detect and correctly position in depth all the features and attributes observed in the 3D dataset if only a 2D seismic survey had been executed. This study should further encourage future mineral exploration programmes to implement, when possible, 3D seismic methods for accurate VMS detection and targeting at depth.

ACKNOWLEDGEMENTS

We thank Somincor-Portugal (a subsidiary of the Lundin Mining Corporation) for providing access to the seismic data and for collaborating with us through the Smart Exploration project. Smart Exploration has received funding from the European Union's Horizon 2020 research and innovation program under grant agreement no. 775971. George. A. Donoso's Ph.D. work is supported by the project. Globe Claritas and Matlab were used for data processing and modelling purposes, the visualization and plotting were done via Generic Mapping Tools (GMT) and GoCAD. We thank the reviewers Sinem Yavuz, Saeid Cheraghi, and the associate editor for their constructive comments on an earlier version of this article.

DATA AVAILABILITY STATEMENT

The reflection seismic data presented are subject to an embargo of 2 years from the date of the publication to allow for commercialization of research findings. They will become available in the Swedish National Data Service (https://www.snd.gu.se).

ORCID

George A. Donoso https://orcid.org/0000-0002-7087-4163
Alireza Malehmir https://orcid.org/0000-0003-1241-2988

REFERENCES

Alonaizi, F., Pevzner, R., Bóna, A., Shulakova, V. & Gurevich, B. (2013) 3D diffraction imaging of linear features and its application to seismic monitoring. *Geophysical Prospecting*, 61, 1206–1217.

Bellefleur, G., Malehmir, A. & Müller, C. (2012) Elastic finite-difference modeling of volcanic-hosted massive sulfide deposits: a case study from Half Mile Lake, New Brunswick, Canada. *Geophysics*, 77, WC25–WC36.

Bellefleur, G., Mueller, C., Snyder, D.B. & Matthews, L. (2004) Downhole seismic imaging of a massive sulfide orebody with mode-converted waves, Halfmile Lake, New Brunswick, Canada. *Geophysics*, 69, 318–329.

Bohlen, T., Müller, C. & Milkereit, B. (2003) Elastic seismic-wave scattering from massive sulfide orebodies: on the role of composition and shape. In: Eaton, D.W., Milkereit, B. & Salisbury, H. (Eds.) *Hardrock seismic exploration*. Houston, TX: SEG, pp. 70–89.

Brodic, B., Malehmir, A., Pacheco, N., Juhlin, C., Dynesius, L., Carvalho, J., van den Berg, J., de Kunder, R., Donoso, G.A., Sjölund, T. & Araujo, V. (2021) Innovative seismic imaging of VMS deposits, Neves-Corvo, Portugal - Part I: in-mine Array. *Geophysics*, 86, B165–B179.

Carvalho, J., Dias, P., Reveaux, C., Matos, J.X., Araújo, V., Inverno, C., Marques, F., Donoso, G.A., Pacheco, N., Morais, I., Albardeiro, L., Batista, M.J., Malehmir, A., Spicer, B. & Oliveira, D. (2021) A drill-hole, geological and geophysical data-based 3D model for target generation in Neves-Corvo mine region, Portugal. *International Journal of Earth Sciences*, 111, 403–424.

Cheraghi, S., Malehmir, A., Bellefleur, G., Bongajum, E. & Bastani, M. (2013) Scaling behavior and the effects of heterogeneity on shallow seismic imaging of mineral deposits: a case study from Brunswick No. 6 mining area, Canada. *Journal of Applied Geophysics*, 90, 1–18.

Cordsen, A., Galbraith, M. & Peirce, J. (2000) *Planning land 3-D seismic surveys*. Houston, TX: Society of Exploration Geophysicists, 217 pp.

Deregowski, S.M. (1986) What is DMO? *First Break*, 4, 7–24.

Donoso, G.A., Malehmir, A., Pecheco, N., Araujo, V., Penney, M., Carvalho, J., Spicer, B. & Beach, S. (2020) Potential of legacy 2D seismic data for deep-targeting and structural imaging at the Neves-Corvo massive sulphide-bearing site, Portugal. *Geophysical Prospecting*, 68, 44–61.

Donoso, G.A., Malehmir, A., Brodic, B., Pacheco, N., Carvalho, J. & Araujo, V. (2021) Innovative seismic imaging of VMS deposits, Neves Corvo, Portugal – Part II: surface array. *Geophysics*, 86, B181–B191.

Eaton, D., Milkereit, B. & Salisbury, M. (2003) Hardrock seismic exploration: mature technologies adapted to new exploration targets. In: *Foreword to Hardrock seismic exploration*. Houston, TX: SEG, Vol. 10, pp. 1–6.

Herron, D.A. & Smith, T.E. (2019) Practical aspects of working with 2D migrated seismic data. *Interpretation*, 7, 1A–T725.

Keller, J. (1962) Geometrical theory of diffraction. *Journal of the Optical Society of America*, 52, 116–130.

Klem-Musatov, K. (1994) *Theory of seismic diffractions*. Houston, TX: Society of Exploration Geophysicists.

Malehmir, A. & Bellefleur, G. (2009) 3D seismic reflection imaging of volcanic-hosted massive sulfide deposits: insights from

13652478, 0, Downloaded from https://onlinelibrary.wiley.com/doi/10.1111/1365-2478.13269 by Cochrane Portugal, Wiley Online Library on [14/12/2022]. See the Terms and Conditions (https://onlinelibrary.wiley.com/terms-and-conditions) on Wiley Online Library for rules of use; OA articles are governed by the applicable Creative Commons License

reprocessing Halfmile Lake data, New Brunswick, Canada. *Geophysics*, 74(6), B209–B219.

Malehmir, A., Bellefleur, G., Koivisto, E. & Juhlin, C. (2017) Pros and cons of 2D vs 3D seismic mineral exploration surveys. *First Break*, 35, 49–55.

Malehmir, A., Durrheim, R., Bellefleur, G., Urosevic, M., Juhlin, C., White, D., Milkereit, B. & Campbell, G. (2012) Seismic methods in mineral exploration and mine planning: a general overview of past and present case histories and a look into the future. *Geophysics*, 77, WC173–WC190.

Markovic, M., Malehmir, R. & Malehmir, A. (2022), Diffraction pattern recognition using deep semantic segmentation. *Near Surface Geophysics*, 20, 507–518.

Matthews, L. (2002) Base metal exploration: looking deeper and adding value with seismic data. *Canadian Society of Exploration Geophysicists Recorder*, 27, 37–43.

Mendes, M., Pereira, Z., Matos, J.X., Morais, I., Albardeiro, L., Solá, R., Pacheco, N. & Araújo, V. (2018) New preliminary data from Phyllite-Quartzite Formation age based on palynomorphs from Middle-Upper Devonian in Neves-Corvo mine region, Iberian Pyrite Belt (Portugal). In: *Proceedings of X Congresso Nacional de Geologia, S. Miguel Açores. Vulcânica, II. Sao Miguel: Açores*. Açores, Portugal: Instituto de Investigação em Vulcanologia e Avaliação de Riscos. pp. 191–92.

Milkereit, B., Eaton, D.W., Wu, J., Perron, G., Salisbury, M.H., Berrer, E. et al. (1996) Seismic imaging of massive sulphide deposits: part II. Reflection seismic profiling. *Economic Geology*, 91, 829–834.

Milkereit, B., Berrer, E.K., King, A.R. et al. (2000) Development of 3-D seismic exploration technology for deep nickel-copper deposits—a case history from the Sudbury basin, Canada. *Geophysics*, 65, 1890–1899.

Oliveira, J.T., Pereira, Z., Carvalho, P., Pacheco, N. & Korn, D. (2004) Stratigraphy of the tectonically imbricated lithological succession of the Neves-Corvo Mine region, Iberian Pyrite Belt. Implications for the regional basin dynamics. *Mineralium Deposita*, 39, 422–36.

Oliveira, J., Rosa, C., Pereira, Z., Rosa, D., Matos, J., Inverno, C. & Andersen, T. (2013) Geology of the Rosário-Neves Corvo antiform, Iberian Pyrite Belt, Portugal: new insights from physical volcanology, palynostratigraphy and isotope geochronology studies. *Mineralium Deposita*, 48, 749–766.

Pereira, Z., Matos, J., Solá, A., Batista, M., Salgueiro, R., Rosa, C., Albardeiro, L., Mendes, M., Morais, I., Oliveira, D., Pacheco, N., Araújo, V., Branco, J., Neto, R., Amaral, J., Inverno, C. & Oliveira, J. (2021) Geology of the recently discovered massive and stockwork sulphide mineralization at Semblana, Rosa Magra and Monte Branco, Neves–Corvo mine region, Iberian Pyrite Belt, Portugal. *Geological Magazine*, 158, 1253–1268.

Pereira, Z., Matos, J.X., Fernandes, P. & Oliveira, J.T. (2008) Palynostratigraphy and systematic palynology of the Devonian and Carboniferous successions of the South Portuguese Zone, Portugal. *Memorias INETI*, 34, 1–176.

Relvas, J., Barriga, F., Pinto, A., Ferreira, A., Pacheco, N., Noiva, P., Barriga, G., Baptista, R., Carvalho, D., Oliveira, V., Munhá, J. & Hutchinson, R. (2002) The Neves-Corvo deposit, Iberian Pyrite Belt, Portugal: impacts and Future, 25 Years after the discovery. *SEG Special Publication*, 9, 155–76.

Rochlin, I., Landa, E. & Keydar, S. (2021) Detection of subsurface lineaments using edge diffraction. *Geophysics*, 86, 1MJ–WA152.

Salisbury, M.H., Harvey, C.W. & Matthews, L. (2003) The acoustic properties of ores and host rocks in hardrock terranes. In: (2003) The acoustic properties of ores and host rocks in hardrock terranes. In: Eaton, D.W., Milkereit, B. & Salisbury, M.H. (Eds.) *Hardrock seismic exploration*. Houston, TX: Society of Exploration Geophysicists, pp. 9–19.

Salisbury, M.H., Milkereit, B., Ascough, G., Adair, R., Matthews, L., Schmitt, D.R., Mwenifumbo, J., Eaton, D.W. & Wu, J. (2000) Physical properties and seismic imaging of massive sulphides. *Geophysics*, 65, 1882–1889.

Stevenson, F. & Durrheim, R.J. (1997) Reflection seismics for gold, platinum and base metal exploration and mining in southern Africa. In: Gubins, A.G. (Ed.) *Proceedings of Exploration 97: Fourth Decennial International Conference on Mineral exploration and Development*. Toronto, Canada: Prospectors and Developers Association of Canada, pp. 391–398.

Streel, M. (2009) Upper Devonian miospore and conodont zone correlation in western Europe. In: Königshof, P. (Ed.) *Devonian change: Case studies in palaeogeography and palaeoecology*. Geological Society of London, Special Publication no. 314. London: Geological Society of London, pp. 163–76.

Streel, M., Brice, D. & Mistiaen, B. (2006) Strunian. *Geologica Belgica*, 9, 105–9.

Urosevic, M., Bhat, G. & Grochau, M. (2012) Targeting nickel sulfide deposits from 3D seismic reflection data at Kambalda, Australia. *Geophysics*, 77, WC123–WC132.

Vermeer, G.J.O. (1998) 3-D symmetric sampling. *Geophysics*, 63, 1629–1647.

West, D. & Penney, M. (2017) Brownfields and Beyond – Undercover at Neves Corvo, Portugal. In: Gubins, A.G. (Ed.) *Proceedings of Exploration 17. Sixth Decennial International Conference on Mineral Exploration*. Toronto, Canada: Prospectors and Developers Association of Canada, pp. 291–304.

Wu, J., Milkereit, B. & Boerner, D.E. (1995) Seismic imaging of the enigmatic Sudbury structure. *Journal of Geophysical Research: Solid Earth*, 100, 4117–4130.

Yavuz, S. (2015) *Seismic characterization of volcanogenic massive sulfides – The Semblana orebody, Portugal*. Ph.D. thesis, Curtin University.

Yavuz, S., Kinkela, J., Dzunic, A., Penney, M., Neto, R., Araujo, V., Ziramov, S., Pevzner, R. & Urosevic, M. (2015) Physical property analysis and preserved relative amplitude processed seismic imaging of volcanogenic massive sulfides—a case study from Neves–Corvo, Portugal. *Geophysical Prospecting*, 63, 798–812.

Yilmaz, O. (2001) *Seismic data analysis*. Tulsa, OK: Society of Exploration Geophysicists, 526 pp.

How to cite this article: Donoso, G.A., Malehmir, A., Carvalho, J. & Araujo, V. (2022) 3D reflection seismic imaging of volcanogenic massive sulphides at Neves-Corvo, Portugal. *Geophysical Prospecting*, 1–16. https://doi.org/10.1111/1365-2478.13269

13652478, 0, Downloaded from https://onlinelibrary.wiley.com/doi/10.1111/1365-2478.13269 by Cochrane Portugal, Wiley Online Library on [14/12/2022]. See the Terms and Conditions (https://onlinelibrary.wiley.com/terms-and-conditions) on Wiley Online Library for rules of use; OA articles are governed by the applicable Creative Commons License